Dynamical Architecture and Long-Term Stability of the β Pictoris Three-Planet System, and Safe Havens for a Hidden Fourth Planet

July 21, 2026

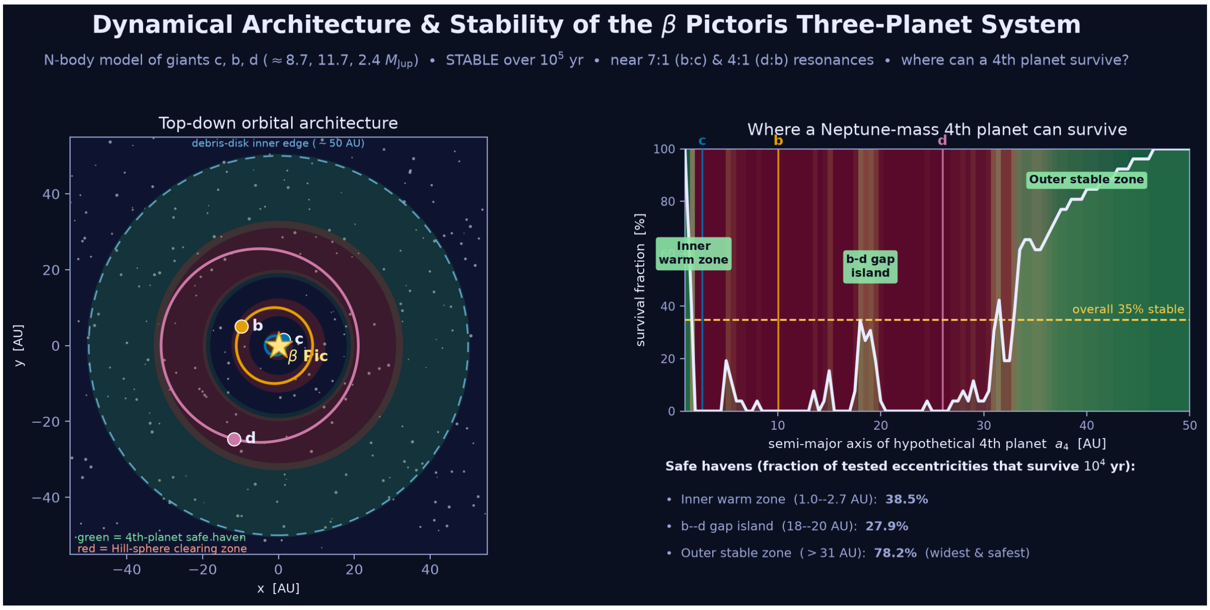

Figure 1: Graphical abstract. *Left:* face-on (top-down) orbital map of the β Pictoris system. Three giant planets—β Pic c ($\approx 8.7\,M_{\rm Jup}$), β Pic b ($\approx 11.7\,M_{\rm Jup}$) and the newly directly-imaged β Pic d ($\approx 2.4\,M_{\rm Jup}$)—are shown with their eccentric orbits; green annuli mark regions where an unseen fourth planet can survive and red annuli mark the Hill-sphere clearing zones of the giants. The dashed circle at 50 AU is the debris-disk inner edge. *Right:* radial survival profile $f_{\rm stable}(a_4)$ from a 99×26 N-body grid sweep, showing three distinct safe havens—an inner warm zone, a narrow island inside the b–d gap, and a wide outer stable zone beyond 31 AU.

Executive Summary

We construct a self-consistent N-body model of the β Pictoris planetary system incorporating all three known giant planets—the long-known imaged giant β Pic b, the radial-velocity/interferometric giant β Pic c, and the recently directly-imaged, lower-mass giant β Pic d ($\approx 2.4\,M_{\rm Jup}$)—orbiting a $1.79\,M_\odot$ A-type star of age ~ 20 Myr. Integrating the nominal three-planet configuration with the high-order adaptive integrator IAS15, we find the system to be **dynamically stable**: there are no orbit crossings, no ejections, and the semi-major axes exhibit only bounded oscillations (net drift $\lesssim 6 \times 10^{-5}$) while relative energy is conserved to $\sim 10^{-14}$. The planets sit *near*, but not precisely in, low-order mean-motion resonances—$P_b/P_c \approx 7.2$ (near 7:1) and $P_d/P_b \approx 4.16$ (near 4:1)—and are separated by $\gtrsim 6.5$ mutual Hill radii, comfortably above the classical two-planet Hill-stability threshold. We then ask where a fourth, as-yet-undetected Neptune-mass planet ($\approx 17\,M_\oplus$) could hide. A 2,574-cell grid sweep over semi-major axis (1–50 AU) and eccentricity (0–0.5) reveals three robust **safe havens**: (i) an inner warm zone interior to β Pic c (1.0–2.7 AU, $\sim 38\%$ survival), (ii) a narrow island within the b–d gap (18–20 AU, $\sim 28\%$), and (iii) a broad, benign outer zone beyond ~ 31 AU inward of the debris disk ($\sim 78\%$ survival). Overall

34.8% of tested orbits survive. These results delineate the regions of orbital "real estate" still available to an undiscovered planet and provide dynamically motivated targets for future high-contrast imaging and astrometry. The dominant uncertainty is the poorly constrained eccentricity of β Pic d, which we treat explicitly as a caveat.

1 Introduction

β Pictoris is arguably the most influential young planetary system in the study of planet formation. Its edge-on circumstellar disk was the first debris disk ever resolved in scattered light (Smith and Terrile, 1984), and mid-infrared imaging soon revealed a warp and a central asymmetry (Lagage and Pantin, 1994) that secular perturbation theory attributed to an unseen planet on an inclined orbit years before any planet was detected (Mouillet et al., 1997). That prediction was spectacularly confirmed when a giant planet, β Pic b, was first glimpsed in the disk (Lagrange et al., 2009) and subsequently confirmed as an orbiting companion through its motion between epochs (Lagrange et al., 2010). The host is a member of the eponymous β Pictoris Moving Group (Zuckerman et al., 2001), whose age has been refined to $\sim$ 18–23 Myr using lithium depletion, isochrones, and dynamical traceback (Mamajek and Bell, 2014; Miret-Roig et al., 2020). At such a youth the system is still in the throes of assembling and clearing its planetary architecture, making it a natural laboratory for the dynamics of young, massive, wide-orbit giant planets.

The system has grown steadily more complex. Precision radial velocities revealed a second, inner giant, β Pic c, whose signal was disentangled from stellar activity (Lagrange et al., 2019, 2020), and which was then directly confirmed and characterized through VLTI/GRAVITY interferometry (Nowak et al., 2020). Combining relative astrometry, radial velocities, and the Hipparcos–Gaia proper-motion anomaly has yielded increasingly precise *dynamical* masses for both giants: β Pic b at ≈ 11–$13\,M_{\rm Jup}$ and β Pic c at ≈ 8–$9\,M_{\rm Jup}$ (Snellen and Brown, 2018; GRAVITY Collaboration et al., 2020; Lagrange et al., 2020; Brandt et al., 2021; Lacour et al., 2021), with the stellar mass itself pinned near $1.8\,M_\odot$ from asteroseismology and dynamics (Wang et al., 2016; Currie et al., 2011). Independently, the debris disk continues to encode the gravitational fingerprints of these planets: mid-plane warps, scattered-light asymmetries, and the striking "CO clumps" mapped by ALMA all point to sculpting by massive perturbers and possibly by additional, undetected bodies (Dent et al., 2014; Nesvold and Kuchner, 2015; Kenworthy et al., 2021).

Most recently, the census has expanded to a third planet. A lower-mass giant, β Pic d—with a mass of only $\approx 2.4\,M_{\rm Jup}$, several times lighter than its siblings—has been characterized on a wide orbit interior to the debris disk (Lacquement et al., 2025). The arrival of a directly-constrained third planet transforms β Pictoris from a two-planet problem into a genuinely multi-planet dynamical system, and it sharpens two long-standing questions. First, is the observed three-giant configuration dynamically self-consistent and stable over the system's lifetime, given the near-resonant period ratios and the substantial planet masses? Second, given the gaps between the known giants and the empty region interior to the debris disk, *where could an additional, smaller planet still be hiding* without having already been ejected or having disrupted the observed architecture?

These questions are not unique to β Pictoris. The four-planet system HR 8799 provides the closest analog of a tightly packed, massive, wide-orbit multiple, and its survival is understood only in terms of a resonant, phase-protected chain (Marois et al., 2008, 2010; Goździewski and Migaszewski, 2020; Fabrycky and Murray-Clay, 2010). Large high-contrast imaging surveys such as GPIES and SHINE have shown that such systems are rare but real, and that the occurrence of wide giant planets around young intermediate-mass stars is non-negligible (Nielsen et al., 2019; Vigan et al., 2021). The formation pathway of these wide giants—core accretion pushed to large separations versus disk gravitational instability—remains actively debated (Boss, 1997; Rafikov, 2005; Kratter et al., 2010; Dodson-Robinson et al., 2009), and the host's slightly super-solar metallicity offers an additional clue (Vandal et al., 2020). Throughout, we anchor the observed and derived properties of the system against the NASA Exoplanet Archive (Akeson et al., 2013), which curates the published orbital and physical parameters for all three β Pictoris planets.

In this report we (i) assemble a consistent set of adopted parameters for the three known giants (Section 2); (ii) verify the dynamical stability of the nominal three-planet configuration with direct N-body integration (Section 3, Section 4); (iii) map the orbital architecture, including Hill-sphere clearing zones and the near-resonant structure (Section 5); and (iv) conduct a systematic grid search for the regions in which an unseen Neptune-mass fourth planet could survive (Section 6). We accompany the static figures with a self-contained interactive orbit simulator (Section 7). We close with a discussion of resonances and Hill boundaries (Section 8) and an explicit statement of caveats—foremost the eccentricity of β Pic d—in Section 9.

2 Adopted System Parameters

Table 1 lists the parameters adopted for the nominal model. Masses and semi-major axes are drawn from the recent literature on the dynamical characterization of the system (Brandt et al., 2021; Lacour et al., 2021; Nowak et al., 2020; Lacquement et al., 2025) and cross-checked against the NASA Exoplanet Archive (Akeson et al., 2013). Because the disk—and hence the planetary orbits—is seen nearly edge-on, all three planets are assigned inclinations near 89°, consistent with the coplanar, disk-embedded geometry inferred from imaging and interferometry (GRAVITY Collaboration et al., 2020; Nowak et al., 2020). Eccentricities are modest for the two massive inner giants and are set to $e_c = 0.307$ and $e_b = 0.105$; for the lower-mass outer planet we adopt a nominal $e_d = 0.19$, while emphasizing (Section 9) that this value is the least certain input to the model. Pericentre and apocentre distances (q, Q) and the instantaneous Hill radius $R_{\mathrm{H}} = a(1-e)\,[m/(3M_\odot)]^{1/3}$ follow directly from these elements.

Table 1: Adopted parameters for the β Pictoris system. The host star mass is $M_\star = 1.789\,M_\odot$. Masses are given in Jupiter masses and (in parentheses) Earth masses; q and Q are pericentre and apocentre; R_{H} is the instantaneous Hill radius at pericentre. Orbital periods follow from Kepler's third law.

Planet	Mass [M_{Jup}]	($M_\oplus$)	a [AU]	e	i [deg]	P [yr]	q, Q [AU]	R_{H} [AU]
c	8.70	(2765)	2.700	0.307	88.93	3.31	1.87, 3.53	0.31
b	11.73	(3728)	10.070	0.105	88.99	23.82	9.01, 11.13	1.28
d	2.40	(763)	26.000	0.190	89.00	99.06	21.06, 30.94	1.96

A first, purely geometric assessment of stability comes from the planetary spacing measured in *mutual* Hill radii, $R_{\mathrm{H}}^{\mathrm{m}} = \frac{1}{2}(a_i + a_j)\,[(m_i + m_j)/(3M_\odot)]^{1/3}$, and the associated dimensionless separation $\Delta_{ij} = (a_j - a_i)/R_{\mathrm{H}}^{\mathrm{m}}$. We find $\Delta_{cb} \approx 7.5$ and $\Delta_{bd} \approx 6.5$, both comfortably above the $\Delta \gtrsim 2\sqrt{3} \approx 3.46$ Hill-stability boundary for isolated pairs (Gladman, 1993) and near the empirical $\Delta \gtrsim 7$–9 regime associated with long-lived multi-planet spacings (Chambers et al., 1996; Smith and Lissauer, 2009; Pu and Wu, 2015). The near-resonant period ratios (Table 2) add an important nuance to this picture, which we return to in Section 8.

Table 2: Period ratios of adjacent and non-adjacent planet pairs and their proximity to low-order mean-motion resonances (MMRs). Offsets are relative to the exact commensurability. The b:c and d:b pairs lie a few percent *wide* of the nearest low-order resonances, whereas d:c falls very close to a high-order 30:1 commensurability.

Pair	Period ratio	Nearest low-order MMR	Offset from exact
b : c	7.197	7 : 1	+2.81%
d : b	4.159	4 : 1	+3.98%
d : c	29.932	30 : 1	−0.23%

3 Methods

3.1 N-body integration

All integrations are performed with the open-source REBOUND package (Rein and Liu, 2012), using astrocentric coordinates with units of years, astronomical units, and solar masses. For the nominal three-planet configuration we employ the IAS15 integrator (Rein and Spiegel, 2015), a 15th-order adaptive Gauss–Radau scheme that is machine-precision accurate and particularly well suited to the moderately eccentric, non-resonant-locked orbits of the β Pictoris giants. The nominal run spans 10^5 yr—approximately 1,010 orbits of the outer planet β Pic d and $\sim 3 \times 10^4$ orbits of the inner planet β Pic c—sampled at 2,000 output epochs. Integrator fidelity is monitored through the fractional energy and angular-momentum errors; we obtain $\max|\Delta E/E_0| \approx 1.5 \times 10^{-14}$ and $\max|\Delta L/L_0| \approx 1.1 \times 10^{-15}$, i.e. round-off limited, so that the dynamical conclusions are not artifacts of integration error.

For the large fourth-planet grid sweep (Section 6) we switch to the hybrid symplectic integrator MERCURIUS (Rein et al., 2019), a modern reimplementation of the Wisdom–Holman/close-encounter hybrid scheme pioneered by MERCURY (Chambers, 1999) and built on the fast WHFast kernel (Rein and Tamayo, 2015). MERCURIUS integrates the well-separated Keplerian motion symplectically with a fixed timestep (here $\Delta t = P_{\min}/25$, one twenty-fifth of the shortest orbital period) while smoothly switching to IAS15 during close encounters, giving the speed required for thousands of integrations without sacrificing accuracy where it matters.

3.2 Stability criteria

An integration is flagged *unstable* and halted if any of the following occurs: (i) **ejection**, defined as a body reaching a stellocentric distance > 200 AU or attaining $e \geq 1$; (ii) a **star-graze/collision**, defined as a pericentre $q < 0.05$ AU or a physical collision with the star; or (iii) a **close encounter** within one Hill radius of any giant. A purely geometric orbit crossing that never leads to a physical close approach is recorded as a non-halting diagnostic, so that bounded, phase-protected orbits—for example those protected by a mean-motion resonance—are correctly retained as stable rather than being spuriously rejected. This choice is deliberately conservative in the direction that matters for a hidden-planet search: we require a candidate orbit to be *genuinely* dynamically survivable, not merely geometrically non-crossing. Our thresholds follow standard practice in the stability-mapping literature (Wisdom, 1980; Deck et al., 2013; Hadden and Lithwick, 2018; Obertas et al., 2017) and are complementary to analytic frameworks such as Hill stability (Gladman, 1993), resonance-overlap chaos (Wisdom, 1980; Deck et al., 2013; Lithwick and Wu, 2011), and angular-momentum-deficit (AMD) stability (Laskar and Petit, 2017; Petit et al., 2017, 2018; Tamayo et al., 2021), against which we interpret the numerical results in Section 8. Chaos indicators such as MEGNO (Cincotta and Simó, 2000) and the broader theory of dynamical chaos in planetary systems (Laskar, 1989; Murray and Dermott,

1999) inform the interpretation but are not required to classify survival on the timescales probed here.

3.3 Fourth-planet grid design

To map the available orbital real estate we insert a single additional test planet of Neptune mass, $m_4 = 0.0537\,M_{\rm Jup} = 17.07\,M_\oplus$, into the fully interacting three-giant system and integrate the resulting four-body problem for 10^4 yr per grid cell. The fourth planet is placed on a near-coplanar orbit ($i_4 = 89°$), with its remaining angles ($\Omega_4 = \omega_4 = M_4 = 0$) fixed by assumption—an unavoidable simplification we flag explicitly in Section 9. We scan a 99×26 grid: semi-major axis a_4 over 99 values from 1 to 50 AU and eccentricity e_4 over 26 values from 0 to 0.5, for a total of 2,574 independent integrations. For each cell we record the survival time, the final classification (stable, orbit-crossing, ejected, star-collision, or planet-collision), and the run of the fourth planet's semi-major axis and eccentricity. From the resulting survival matrix we derive the radial survival profile $f_{\rm stable}(a_4)$—the fraction of tested eccentricities that survive at each semi-major axis—which underpins the safe-haven analysis and the graphical abstract (Figure 1).

4 Stability of the Nominal Three-Planet System

The nominal configuration is dynamically stable over the full 10^5 yr integration. No pair of planets ever crosses orbits, no body is ejected or driven onto the star, and the verdict returned by every stability test is unambiguous. Figure 2 shows the time evolution of the osculating orbital elements. The semi-major axes are essentially flat: the net fractional drift over the whole run is $|\Delta a/a| \lesssim 6 \times 10^{-5}$ for all three planets, far below the 10^{-2} threshold that would signal a slow instability. What oscillation there is (up to $\sim 15\%$ peak-to-peak in the instantaneous a near the resonant forcing) is *bounded and periodic*, the classic signature of near-resonant but non-disruptive secular and mean-motion interactions rather than a random walk toward instability.

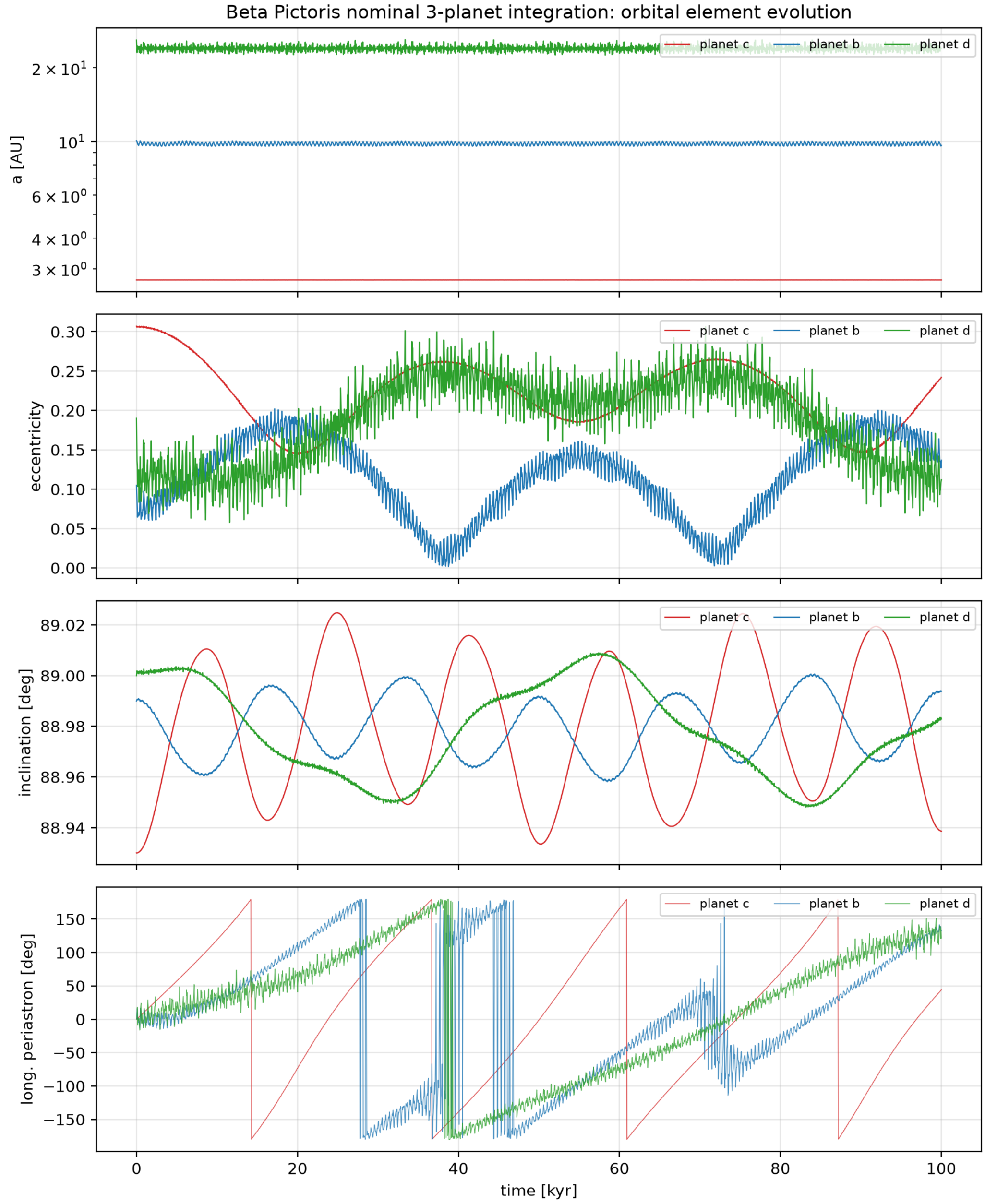

Figure 2: Time evolution of the osculating orbital elements—semi-major axis a, eccentricity e, and inclination i—of the three β Pictoris giants over the 10^5 yr nominal integration with IAS15. All elements oscillate within bounded ranges; the net secular drift in a is negligible ($\lesssim 6 \times 10^{-5}$), the hallmark of a dynamically stable, phase-protected configuration.

The eccentricities librate within secure bounds—$e_c \in [0.14, 0.31]$, $e_b \in [0.00, 0.20]$, $e_d \in [0.06, 0.31]$—exchanging angular momentum in the manner expected of a coupled secular (Laplace–Lagrange) system (Murray and Dermott, 1999), while the inclinations remain tightly clustered near 89°, confirming that the coplanar, disk-embedded assumption is internally consistent and self-maintaining. Crucially, the eccentricity excursions never bring any pair of orbits into contact: even at maximum eccentricity the apocentre of the inner member of each pair stays well interior to the pericentre of the outer member.

Figure 3 documents the integrator's fidelity. The relative energy error remains at the 10^{-14} level and the angular-momentum error at 10^{-15} throughout, confirming that the smooth, bounded element evolution in Figure 2 reflects the true dynamics of the model rather than accumulated numerical error. Taken together, these diagnostics establish a firm baseline: the three *known* planets form a stable system, so any hidden fourth planet must be accommodated *within* this already-constrained architecture.

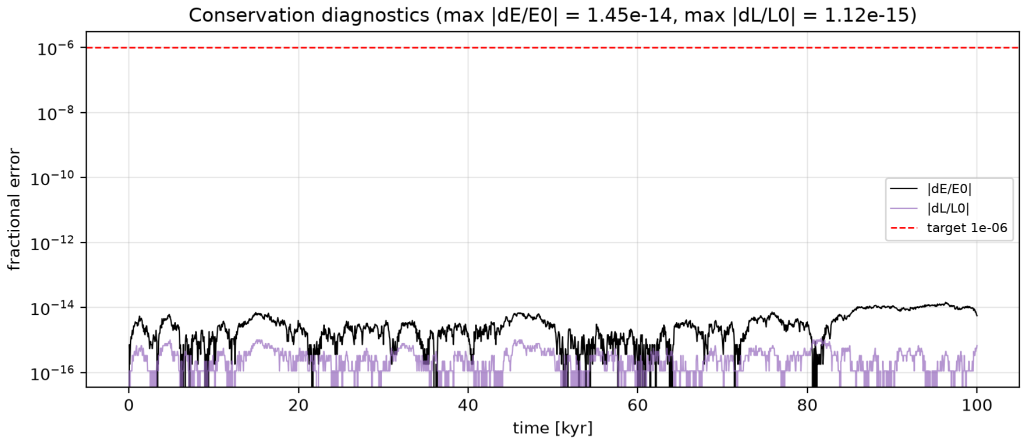

Figure 3: Conservation diagnostics for the nominal integration. The fractional energy error $|\Delta E/E_0|$ (left) stays at $\sim 10^{-14}$ and the angular-momentum error $|\Delta L/L_0|$ (right) at $\sim 10^{-15}$ over the entire span, i.e. the run is round-off limited. The dynamical conclusions are therefore not artifacts of integration error.

5 Orbital Architecture and Hill-Sphere Structure

Figure 4 presents a top-down, face-on rendering of the system that makes the scale hierarchy immediately legible. The three giants trace nested eccentric ellipses whose apsides are drawn with their true relative sizes; around each planet's orbit lies a *Hill-clearing annulus* (shaded), spanning from the planet's pericentre minus its Hill radius to its apocentre plus its Hill radius, within which no long-lived low-mass body can reside. For the adopted parameters these exclusion annuli span roughly 1.6–3.8 AU (planet c), 7.7–12.4 AU (planet b), and 19.1–32.9 AU (planet d). The gaps *between* these annuli—interior to c, between c and b, between b and d, and exterior to d out to the debris disk—are precisely the regions where an additional planet might survive, and they motivate the grid search of Section 6.

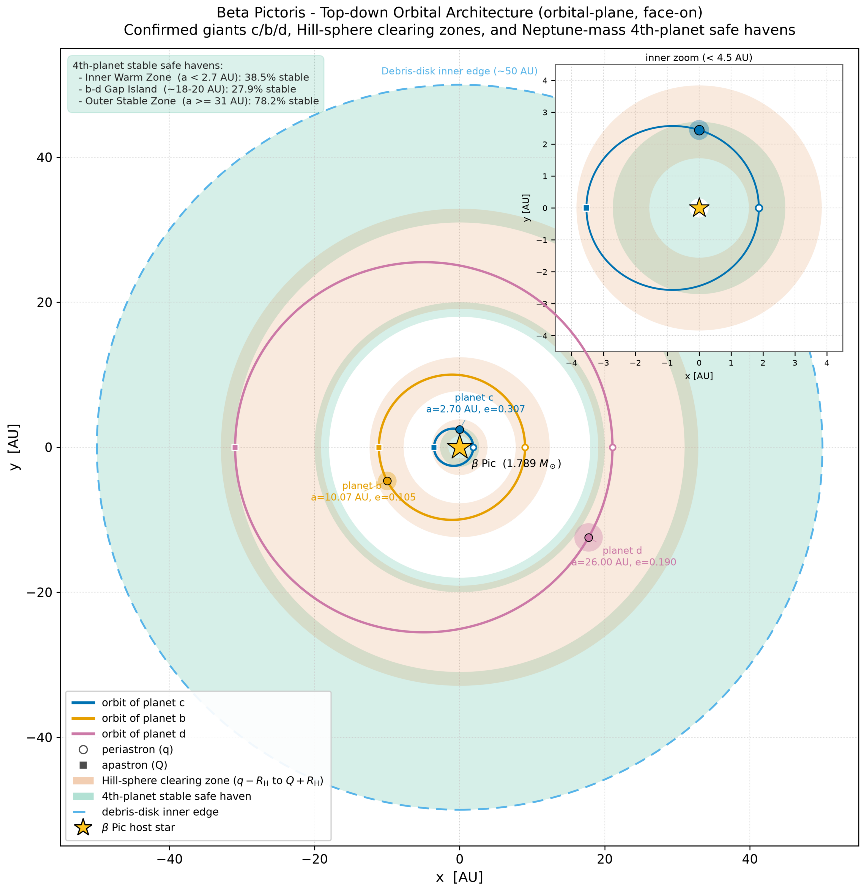

Figure 4: Top-down (face-on) view of the β Pictoris orbital architecture. Solid ellipses are the orbits of planets c, b, and d; shaded annuli are the Hill-sphere clearing zones, within which a small body would encounter a giant within one Hill radius. The dashed circle marks the debris-disk inner edge near 50 AU. Note the wide, clear gaps interior to c, between b and d, and exterior to d—the candidate regions for a hidden fourth planet.

Figure 5 complements the top-down map with a quantitative summary of the architecture: the radial placement of each planet with its pericentre–apocentre excursion, the mass hierarchy, the Hill-radius and mutual-Hill spacing, and the location of the debris disk. The system is strongly ordered by mass in its inner region—the two most massive giants (b and c) dominate the dynamics inside 12 AU—while the lighter planet d governs a much larger volume at wide separation simply by virtue of its greater orbital radius (its Hill radius, 1.96 AU, exceeds that of the more massive c because Hill radius scales with a). The debris disk begins just beyond planet d's apocentre, consistent with the picture in which the outermost planet defines the inner edge of the planetesimal belt (Dent et al., 2014; Nesvold and Kuchner, 2015; Kenworthy et al., 2021).

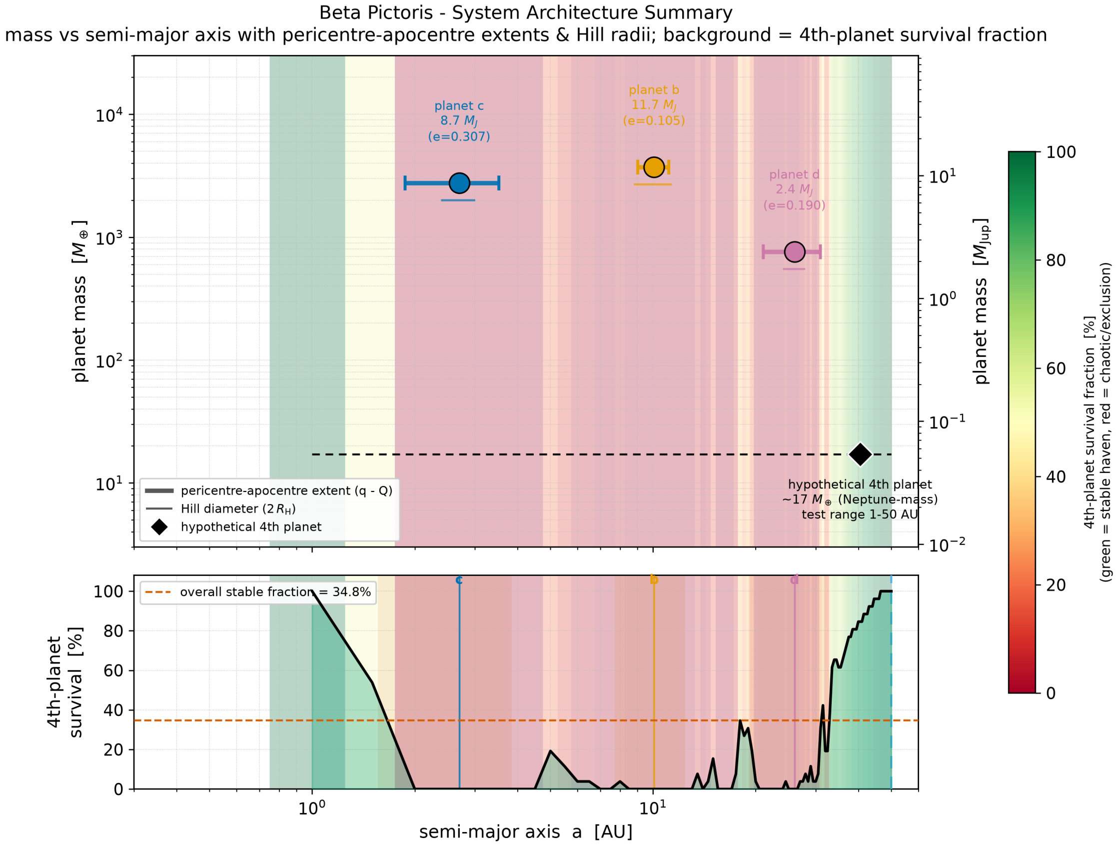

Figure 5: Quantitative summary of the β Pictoris architecture: radial placement and pericentre–apocentre spans of the three giants, their masses and Hill radii, the mutual Hill separations of adjacent pairs, and the debris-disk inner edge. Planet d, though the least massive, commands the largest Hill radius owing to its wide orbit.

6 Safe Havens for a Hidden Fourth Planet

We now turn to the central question: where could an as-yet-unseen Neptune-mass planet survive within this architecture? Figure 6 shows the survival-time heatmap over the full (a_4, e_4) grid, and Figure 7 classifies the fate of every cell. Of the 2,574 integrations, 896 (34.8%) survive the full 10^4 yr as bounded, non-encountering orbits; the remainder are dominated by orbit-crossing/close-encounter outcomes (1,652 cells), with a small number of outright ejections (23) and star-grazing collisions (3), and no planet–planet collisions. The overall event tally is collected in Table 3.

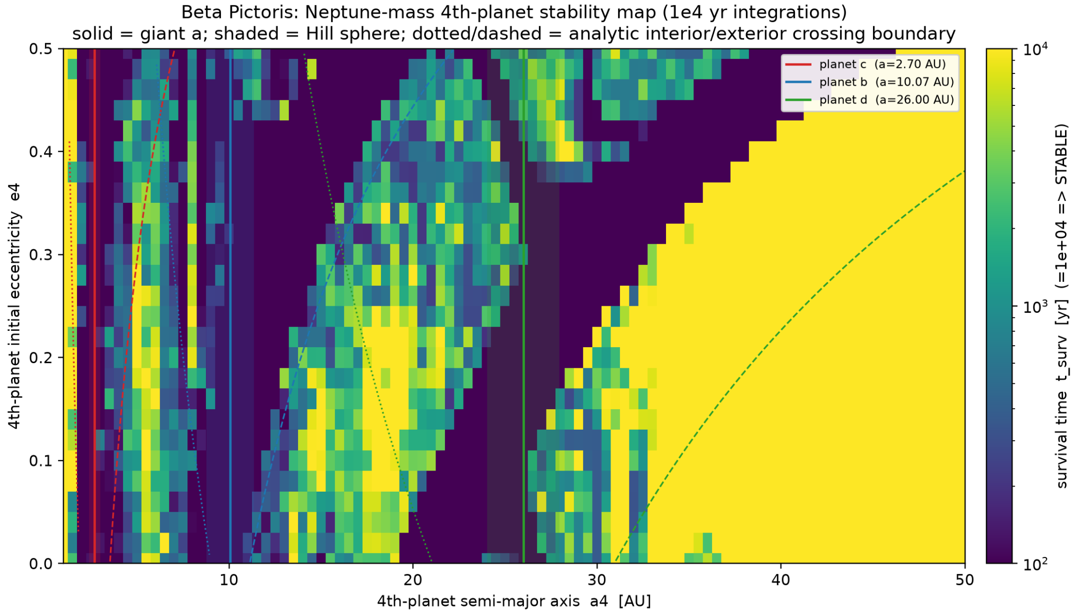

Figure 6: Survival-time heatmap for a Neptune-mass ($\approx 17\,M_\oplus$) fourth planet as a function of its semi-major axis a_4 (horizontal) and eccentricity e_4 (vertical), from 2,574 N-body integrations of the four-body system with MERCURIUS. Bright regions survive the full 10^4 yr; dark regions destabilize. Vertical dark stripes mark the Hill-clearing zones of the three known giants; broad bright columns mark the safe havens.

Figure 7: Outcome classification of each grid cell: stable (survives), orbit-crossing/close encounter, ejected, or star-collision. The stable cells cluster into three coherent regions in a_4—interior to planet c, a narrow island inside the b–d gap, and a broad zone exterior to planet d—rather than being scattered, indicating that survival is governed by the system's global architecture rather than by chance.

Three coherent safe havens emerge, and they are the same three features visible in the radial survival profile of the graphical abstract (Figure 1, right panel):

1. **Inner warm zone (1.0–2.7 AU; $\sim 38\%$ survival).** Interior to the innermost giant β Pic c, a Neptune-mass planet can persist on low-to-moderate eccentricity orbits. Survival here is limited chiefly by the strong secular forcing and the pericentre excursions of the eccentric planet c ($e_c = 0.307$, $q_c = 1.87$ AU), so the haven is warm, dynamically "busy," and

eccentricity-sensitive, but real.

2. **The b–d gap island (18–20 AU; $\sim 28\%$ survival).** The wide gap between planets b and d is mostly hostile—averaged over the broad 12–21 AU range only $\sim 8\%$ of orbits survive—but survival is not uniform. It concentrates into a narrow island near 18–20 AU, in the "no man's land" between the outer edge of b's Hill-clearing annulus and the inner edge of d's. This island is dynamically delicate and its precise width depends sensitively on the (uncertain) eccentricity of planet d.
3. **Outer stable zone (> 31 AU; $\sim 78\%$ survival).** Beyond planet d's Hill-clearing annulus, and interior to the debris-disk inner edge near 50 AU, lies by far the widest and most benign haven: roughly four out of five tested orbits survive. This region is the strongest candidate location for an undiscovered planet on dynamical grounds alone, and it is spatially coincident with the inner edge of the planetesimal belt that massive perturbers are expected to sculpt (Dent et al., 2014; Nesvold and Kuchner, 2015).

Table 3: Fourth-planet grid sweep: setup, outcome tally, and safe-haven survival fractions. The test planet has mass $m_4 = 17.07\,M_\oplus$ ($0.0537\,M_{\rm Jup}$) and inclination $i_4 = 89°$; each of the 2,574 cells is integrated for 10^4 yr with MERCURIUS.

Grid setup	
Semi-major axis a_4	1–50 AU (99 values)
Eccentricity e_4	0–0.5 (26 values)
Total integrations	2,574
Integration span	10^4 yr per cell
Outcome tally	
Stable (survived)	896 (34.8%)
Orbit-crossing / encounter	1,652
Ejected ($r > 200$ AU or $e \geq 1$)	23
Star collision / graze	3
Planet–planet collision	0
Safe-haven survival fractions	
Inner warm zone (1.0–2.7 AU)	38.5%
b–d gap island (18–20 AU)	27.9%
(broad b–d gap, 12–21 AU)	8.3%
Outer stable zone (> 31 AU)	78.2%

7 Interactive Orbit Simulator

To make the architecture explorable rather than merely static, the analysis is accompanied by a self-contained, browser-based orbit simulator delivered as a single HTML5 file (`final/interactive_orbit_simulator.html`). Opening the file in any modern web browser launches an animated, top-down rendering of the three-planet system in which the giants move on their true (scaled) orbits; the viewer can toggle the Hill-clearing annuli, overlay the three safe-haven zones identified in Section 6, and insert a test fourth planet at a chosen semi-major axis and eccentricity to watch its short-term behavior in the context of the known giants. The simulator uses the same adopted parameters as Table 1 and is intended as a companion to Figures 4 and 1, giving an intuitive feel for the resonant, near-commensurable rhythm of the system that the static figures can only summarize.

8 Discussion

8.1 Resonances: near, but not locked

The most striking dynamical feature of β Pictoris is that its giants sit *near* low-order mean-motion resonances without being locked in them (Table 2). The b:c period ratio of 7.20 lies $\sim 2.8\%$ wide of the 7:1 commensurability, and the d:b ratio of 4.16 lies $\sim 4.0\%$ wide of 4:1. This "near-resonant but offset" configuration is common among mature multi-planet systems and is widely interpreted as the fossil of convergent disk migration followed by a small divergence—through tidal or planetesimal interactions—that leaves pairs parked just wide of exact resonance (Lithwick and Wu, 2011; Fabrycky and Murray-Clay, 2010). Whether β Pictoris is truly captured in a high-order resonance or merely near one has real dynamical consequences: a genuine resonant lock provides phase protection that can stabilize otherwise-crossing orbits, exactly as invoked to explain the survival of the closely packed HR 8799 giants (Goździewski and Migaszewski, 2020; Marois et al., 2010; Fabrycky and Murray-Clay, 2010). The bounded, periodic element oscillations we observe in Figure 2—large in amplitude yet drift-free—are consistent with such near-resonant secular coupling. The most intriguing entry in Table 2 is the d:c pair, which sits only 0.23% from an exact 30:1 commensurability; while high-order resonances are individually weak, this proximity is a natural target for the longer, resonance-resolving integrations recommended below.

8.2 Hill spheres and the geometry of exclusion

The safe havens map cleanly onto the Hill-sphere geometry of Section 5. Each giant sweeps clear an annulus extending roughly one Hill radius beyond its pericentre and apocentre, and the stable columns in Figures 6–7 are exactly the complementary gaps. That the surviving cells cluster into three coherent regions, rather than scattering randomly, confirms that survival is set by the global architecture—the interplay of overlapping secular forcing and Hill-sphere clearing—rather than by cell-by-cell happenstance. The adjacent giants themselves are separated by $\Delta_{cb} \approx 7.5$ and $\Delta_{bd} \approx 6.5$ mutual Hill radii, above the analytic Hill-stability limit (Gladman, 1993) and in the empirically long-lived spacing regime (Chambers et al., 1996; Smith and Lissauer, 2009; Pu and Wu, 2015; Obertas et al., 2017). A hidden fourth planet inserted into the outer zone would add a fourth well-separated body to an already comfortably spaced chain, which is precisely why that zone is the most forgiving.

8.3 Where the AMD framework points

Complementary to direct integration, the angular-momentum-deficit (AMD) framework provides an analytic secular criterion for whether a planetary system can undergo orbit crossing (Laskar and Petit, 2017; Petit et al., 2017), extended to account for the destabilizing role of mean-motion resonances (Petit et al., 2018; Tamayo et al., 2021) and the resonance-overlap onset of chaos (Wisdom, 1980; Deck et al., 2013; Hadden and Lithwick, 2018). The low, bounded eccentricities of the known giants imply a modest system AMD, consistent with the numerical stability we find; the same framework predicts that the inner warm zone—where secular forcing from the eccentric planet c is strongest—should be the most eccentricity-sensitive haven, exactly as observed. A full AMD and MEGNO (Cincotta and Simó, 2000) characterization of the safe havens, mapping the chaotic boundaries analytically, is a natural extension of this work.

8.4 The system in context

β Pictoris now joins HR 8799 as one of only a handful of directly-imaged multiple-giant systems (Marois et al., 2008, 2010; Nielsen et al., 2019; Vigan et al., 2021), and its three-planet architecture—two massive inner giants and a lighter, wider third planet interior to a debris belt—offers a valuable second data point for theories of wide-orbit giant formation. Whether these planets formed by core accretion at large separations, by outward scattering, or by disk gravitational instability remains open (Boss, 1997; Rafikov, 2005; Kratter et al., 2010; Dodson-Robinson et al., 2009), and the host's mildly super-solar metallicity (Vandal et al., 2020) is a further clue. Our stability map contributes to this discussion by quantifying which additional bodies the present architecture can dynamically tolerate—information that any formation scenario must ultimately reproduce.

9 Caveats and Limitations

Key Caveats and Limitations

The results above are robust *within the model as posed*, but several inputs and choices limit their reach. We state these plainly rather than burying them.

- **The eccentricity of β Pic d is the dominant uncertainty.** We adopt a nominal $e_d = 0.19$, but this is the least well-constrained parameter in the model. Because planet d is the outermost giant and defines the inner boundary of the widest and most populated safe haven, its eccentricity directly controls the location of the outer haven's inner edge and the width of the delicate b–d gap island. A larger e_d would widen d's Hill-clearing annulus, erode the b–d island, and push the outer safe zone outward; a smaller e_d would do the reverse. The quoted survival fractions for the b–d island in particular should be read as model-dependent.
- **Integration spans probe short-term, not Gyr-scale, stability.** The nominal run covers 10^5 yr and each grid cell 10^4 yr. These spans robustly capture fast, Hill-sphere and resonance-overlap (Lyapunov-timescale) instabilities—which act within 10^3–10^4 orbits—but they do *not* rule out slow, secular or diffusive instabilities that can unfold over 10^6–10^9 yr. The excellent energy conservation ($\sim 10^{-14}$) guarantees numerical fidelity, not dynamical permanence. Extending the survivor set to full system-lifetime ($\sim 20\,$Myr) and Gyr integrations is the essential next step.
- **Unconstrained angles and single-inclination assumption.** The test fourth planet is inserted with fixed nodal, argument-of-pericentre, and mean-anomaly angles ($\Omega_4 = \omega_4 = M_4 = 0$) and a single inclination ($i_4 = 89°$). The true survival fraction should be marginalized over these phases and over a range of mutual inclinations; resonant phase protection in particular can make survival strongly dependent on the initial angles.
- **Fixed giant masses and a coplanar model.** We adopt single-valued masses and a near-coplanar geometry. The dynamical masses of b and c still carry $\sim 10\%$ uncertainties, and modest mutual inclinations—plausible given the observed disk warp—would alter the secular coupling. A Monte Carlo propagation of the observational error bars into the stability map would convert the present deterministic result into a probabilistic one.
- **Test-particle-like treatment of the fourth planet.** At $\sim 17\,M_\oplus$ the fourth planet is light enough that its back-reaction on the giants is small, but not zero; a more massive hidden planet would carve wider exclusion zones and shrink every haven.

10 Conclusions

Direct N-body integration confirms that the three known giant planets of β Pictoris—c, b, and the newly directly-imaged d—form a dynamically stable, near-resonant system with bounded element oscillations, no orbit crossings, and machine-precision energy conservation over 10^5 yr.

Against this stable backdrop, a systematic 2,574-cell grid search for a hidden Neptune-mass fourth planet identifies three coherent safe havens: an inner warm zone interior to planet c (1.0–2.7 AU, $\sim$ 38% survival), a narrow and delicate island within the b–d gap (18–20 AU, $\sim$ 28%), and a broad, benign outer zone between planet d and the debris disk (>31 AU, $\sim$ 78%). The outer zone is the most promising hiding place on dynamical grounds and coincides with the sculpted inner edge of the planetesimal belt. These havens are the empty "real estate" the observed architecture can tolerate, and they translate directly into dynamically motivated search regions for future high-contrast imaging and astrometry. The single most important refinement—because it controls the boundaries of the widest haven—is a better measurement of the eccentricity of β Pic d, followed by extending the survivor integrations to the full system lifetime and marginalizing over orbital phase and mass uncertainties.

References

R. L. Akeson, X. Chen, D. Ciardi, et al. The NASA Exoplanet Archive: Data and Tools for Exoplanet Research. *Publications of the Astronomical Society of the Pacific*, 125(930):989–999, 2013. doi: 10.1086/672273.

Alan P. Boss. Giant Planet Formation by Gravitational Instability. *Science*, 276(5320):1836–1839, 1997. doi: 10.1126/science.276.5320.1836.

G. Mirek Brandt, Timothy D. Brandt, Trent J. Dupuy, Yiting Li, and Daniel Michalik. Precise Dynamical Masses and Orbital Fits for β Pic b and β Pic c. *The Astronomical Journal*, 161 (4):179, 2021. doi: 10.3847/1538-3881/abdc2e.

J. E. Chambers. A hybrid symplectic integrator that permits close encounters between massive bodies. *Monthly Notices of the Royal Astronomical Society*, 304(4):793–799, 1999. doi: 10.1046/j.1365-8711.1999.02379.x.

J.E. Chambers, G.W. Wetherill, and A.P. Boss. The Stability of Multi-Planet Systems. *Icarus*, 119(2):261–268, 1996. doi: 10.1006/icar.1996.0019.

P. M. Cincotta and C. Simó. Simple tools to study global dynamics in non-axisymmetric galactic potentials – I. *Astronomy & Astrophysics Supplement Series*, 147(2):205–228, 2000. doi: 10.1051/aas:2000108.

Thayne Currie, Adam Burrows, Yoichi Itoh, et al. A COMBINED SUBARU/VLT/MMT 1-5 μm STUDY OF PLANETS ORBITING HR 8799: IMPLICATIONS FOR ATMOSPHERIC PROPERTIES, MASSES, AND FORMATION. *The Astrophysical Journal*, 729(2):128, 2011. doi: 10.1088/0004-637X/729/2/128.

Katherine M. Deck, Matthew Payne, and Matthew J. Holman. FIRST-ORDER RESONANCE OVERLAP AND THE STABILITY OF CLOSE TWO-PLANET SYSTEMS. *The Astrophysical Journal*, 774(2):129, 2013. doi: 10.1088/0004-637X/774/2/129.

W. R. F. Dent, M. C. Wyatt, A. Roberge, et al. Molecular Gas Clumps from the Destruction of Icy Bodies in the β Pictoris Debris Disk. *Science*, 343(6178):1490–1492, 2014. doi: 10.1126/science.1248726.

Sarah E. Dodson-Robinson, Dimitri Veras, Eric B. Ford, and C. A. Beichman. THE FORMATION MECHANISM OF GAS GIANTS ON WIDE ORBITS. *The Astrophysical Journal*, 707(1): 79–88, 2009. doi: 10.1088/0004-637X/707/1/79.

Daniel C. Fabrycky and Ruth A. Murray-Clay. STABILITY OF THE DIRECTLY IMAGED MULTIPLANET SYSTEM HR 8799: RESONANCE AND MASSES. *The Astrophysical Journal*, 710(2):1408–1421, 2010. doi: 10.1088/0004-637X/710/2/1408.

Brett Gladman. Dynamics of Systems of Two Close Planets. *Icarus*, 106(1):247–263, 1993. doi: 10.1006/icar.1993.1169.

Krzysztof Goździewski and Cezary Migaszewski. An Exact, Generalized Laplace Resonance in the HR 8799 Planetary System. *The Astrophysical Journal Letters*, 902(2):L40, 2020. doi: 10.3847/2041-8213/abb881.

GRAVITY Collaboration, M. Nowak, S. Lacour, et al. Peering into the formation history of β Pictoris b with VLTI/GRAVITY long-baseline interferometry. *Astronomy & Astrophysics*, 633:A110, 2020. doi: 10.1051/0004-6361/201936898.

Sam Hadden and Yoram Lithwick. A Criterion for the Onset of Chaos in Systems of Two Eccentric Planets. *The Astronomical Journal*, 156(3):95, 2018. doi: 10.3847/1538-3881/aad32c.

M. A. Kenworthy, S. N. Mellon, J. I. Bailey, et al. The β Pictoris b Hill sphere transit campaign. *Astronomy & Astrophysics*, 648:A15, 2021. doi: 10.1051/0004-6361/202040060.

Kaitlin M. Kratter, Ruth A. Murray-Clay, and Andrew N. Youdin. THE RUNTS OF THE LITTER: WHY PLANETS FORMED THROUGH GRAVITATIONAL INSTABILITY CAN ONLY BE FAILED BINARY STARS. *The Astrophysical Journal*, 710(2):1375–1386, 2010. doi: 10.1088/0004-637X/710/2/1375.

S. Lacour, J. J. Wang, L. Rodet, et al. The mass of β Pictoris c from β Pictoris b orbital motion. *Astronomy & Astrophysics*, 654:L2, 2021. doi: 10.1051/0004-6361/202141889.

A. Lacquement, H. Beust, V. Faramaz-Gorka, and Q. Kral. Dynamics of the β Pictoris planetary system and possibility of an additional planet. *Astronomy & Astrophysics*, 694:A236, 2025. doi: 10.1051/0004-6361/202452632.

P. O. Lagage and E. Pantin. Dust depletion in the inner disk of β Pictoris as a possible indicator of planets. *Nature*, 369(6482):628–630, 1994. doi: 10.1038/369628a0.

A.-M. Lagrange, D. Gratadour, G. Chauvin, et al. A probable giant planet imaged in the β Pictoris disk. *Astronomy & Astrophysics*, 493(2):L21–L25, 2009. doi: 10.1051/0004-6361:200811325.

A.-M. Lagrange, M. Bonnefoy, G. Chauvin, et al. A Giant Planet Imaged in the Disk of the Young Star β Pictoris. *Science*, 329(5987):57–59, 2010. doi: 10.1126/science.1187187.

A.-M. Lagrange, Nadège Meunier, Pascal Rubini, et al. Evidence for an additional planet in the β Pictoris system. *Nature Astronomy*, 3(12):1135–1142, 2019. doi: 10.1038/s41550-019-0857-1.

A. M. Lagrange, P. Rubini, M. Nowak, et al. Unveiling the β Pictoris system, coupling high contrast imaging, interferometric, and radial velocity data. *Astronomy & Astrophysics*, 642: A18, 2020. doi: 10.1051/0004-6361/202038823.

J. Laskar. A numerical experiment on the chaotic behaviour of the Solar System. *Nature*, 338 (6212):237–238, 1989. doi: 10.1038/338237a0.

J. Laskar and A. C. Petit. AMD-stability and the classification of planetary systems. *Astronomy & Astrophysics*, 605:A72, 2017. doi: 10.1051/0004-6361/201630022.

Yoram Lithwick and Yanqin Wu. THEORY OF SECULAR CHAOS AND MERCURY'S ORBIT. *The Astrophysical Journal*, 739(1):31, 2011. doi: 10.1088/0004-637X/739/1/31.

Eric E. Mamajek and Cameron P. M. Bell. On the age of the β Pictoris moving group. *Monthly Notices of the Royal Astronomical Society*, 445(3):2169–2180, 2014. doi: 10.1093/mnras/stu1894.

Christian Marois, Bruce Macintosh, Travis Barman, B. Zuckerman, Inseok Song, Jennifer Patience, David Lafrenière, and René Doyon. Direct Imaging of Multiple Planets Orbiting the Star HR 8799. *Science*, 322(5906):1348–1352, 2008. doi: 10.1126/science.1166585.

Christian Marois, B. Zuckerman, Quinn M. Konopacky, Bruce Macintosh, and Travis Barman. Images of a fourth planet orbiting HR 8799. *Nature*, 468(7327):1080–1083, 2010. doi: 10.1038/nature09684.

N. Miret-Roig, P. A. B. Galli, W. Brandner, et al. Dynamical traceback age of the β Pictoris moving group. *Astronomy & Astrophysics*, 642:A179, 2020. doi: 10.1051/0004-6361/202038765.

D. Mouillet, J. D. Larwood, J. C. B. Papaloizou, and A. M. Lagrange. A planet on an inclined orbit as an explanation of the warp in the β Pictoris disc. *Monthly Notices of the Royal Astronomical Society*, 292(4):896–904, 1997. doi: 10.1093/mnras/292.4.896.

Carl D. Murray and Stanley F. Dermott. *Solar System Dynamics*. Cambridge University Press, Cambridge, UK, 1999. doi: 10.1017/CBO9781139174817.

Erika R. Nesvold and Marc J. Kuchner. A SMACK MODEL OF COLLIDING PLANETESIMALS IN THE β PICTORIS DEBRIS DISK. *The Astrophysical Journal*, 815(1):61, 2015. doi: 10.1088/0004-637X/815/1/61.

Eric L. Nielsen, Robert J. De Rosa, Bruce Macintosh, et al. The Gemini Planet Imager Exoplanet Survey: Giant Planet and Brown Dwarf Demographics from 10 to 100 au. *The Astronomical Journal*, 158(1):13, 2019. doi: 10.3847/1538-3881/ab16e9.

M. Nowak, S. Lacour, A.-M. Lagrange, et al. Direct confirmation of the radial-velocity planet β Pictoris c. *Astronomy & Astrophysics*, 642:L2, 2020. doi: 10.1051/0004-6361/202039039.

Alysa Obertas, Christa Van Laerhoven, and Daniel Tamayo. The stability of tightly-packed, evenly-spaced systems of Earth-mass planets orbiting a Sun-like star. *Icarus*, 293:52–58, 2017. doi: 10.1016/j.icarus.2017.04.010.

A. C. Petit, J. Laskar, and G. Boué. AMD-stability in the presence of first-order mean motion resonances. *Astronomy & Astrophysics*, 607:A35, 2017. doi: 10.1051/0004-6361/201731196.

Antoine C. Petit, Jacques Laskar, and Gwenaël Boué. Hill stability in the AMD framework. *Astronomy & Astrophysics*, 617:A93, 2018. doi: 10.1051/0004-6361/201833088.

Bonan Pu and Yanqin Wu. SPACING OFKEPLERPLANETS: SCULPTING BY DYNAMICAL INSTABILITY. *The Astrophysical Journal*, 807(1):44, 2015. doi: 10.1088/0004-637X/807/1/44.

Roman R. Rafikov. Can Giant Planets Form by Direct Gravitational Instability? *The Astrophysical Journal*, 621(1):L69–L72, 2005. doi: 10.1086/428899.

H. Rein and S.-F. Liu. REBOUND: an open-source multi-purposeN-body code for collisional dynamics. *Astronomy & Astrophysics*, 537:A128, 2012. doi: 10.1051/0004-6361/201118085.

Hanno Rein and David S. Spiegel. ias15: a fast, adaptive, high-order integrator for gravitational dynamics, accurate to machine precision over a billion orbits. *Monthly Notices of the Royal Astronomical Society*, 446(2):1424–1437, 2015. doi: 10.1093/mnras/stu2164.

Hanno Rein and Daniel Tamayo. whfast: a fast and unbiased implementation of a symplectic Wisdom–Holman integrator for long-term gravitational simulations. *Monthly Notices of the Royal Astronomical Society*, 452(1):376–388, 2015. doi: 10.1093/mnras/stv1257.

Hanno Rein, David M Hernandez, Daniel Tamayo, Garett Brown, Emily Eckels, Emma Holmes, Michelle Lau, Réjean Leblanc, and Ari Silburt. Hybrid symplectic integrators for planetary dynamics. *Monthly Notices of the Royal Astronomical Society*, 485(4):5490–5497, 2019. doi: 10.1093/mnras/stz769.

Andrew W. Smith and Jack J. Lissauer. Orbital stability of systems of closely-spaced planets. *Icarus*, 201(1):381–394, 2009. doi: 10.1016/j.icarus.2008.12.027.

Bradford A. Smith and Richard J. Terrile. A Circumstellar Disk Around β Pictoris. *Science*, 226(4681):1421–1424, 1984. doi: 10.1126/science.226.4681.1421.

I. A. G. Snellen and A. G. A. Brown. The mass of the young planet Beta Pictoris b through the astrometric motion of its host star. *Nature Astronomy*, 2(11):883–886, 2018. doi: 10.1038/s41550-018-0561-6.

Daniel Tamayo, Norman Murray, Scott Tremaine, and Joshua Winn. A Criterion for the Onset of Chaos in Compact, Eccentric Multiplanet Systems. *The Astronomical Journal*, 162(5):220, 2021. doi: 10.3847/1538-3881/ac1c6a.

Thomas Vandal, Julien Rameau, and René Doyon. Dynamical Mass Estimates of the β Pictoris Planetary System through Gaussian Process Stellar Activity Modeling. *The Astronomical Journal*, 160(5):243, 2020. doi: 10.3847/1538-3881/abba30.

A. Vigan, C. Fontanive, M. Meyer, et al. The SPHERE infrared survey for exoplanets (SHINE). *Astronomy & Astrophysics*, 651:A72, 2021. doi: 10.1051/0004-6361/202038107.

Jason J. Wang, James R. Graham, Laurent Pueyo, et al. THE ORBIT AND TRANSIT PROSPECTS FOR β PICTORIS b CONSTRAINED WITH ONE MILLIARCSECOND ASTROMETRY. *The Astronomical Journal*, 152(4):97, 2016. doi: 10.3847/0004-6256/152/4/97.

J. Wisdom. The resonance overlap criterion and the onset of stochastic behavior in the restricted three-body problem. *The Astronomical Journal*, 85:1122, 1980. doi: 10.1086/112778.

B. Zuckerman, Inseok Song, M. S. Bessell, and R. A. Webb. The β Pictoris Moving Group. *The Astrophysical Journal*, 562(1):L87–L90, 2001. doi: 10.1086/337968.